Journal of Photochemistry and Photobiology A: Chemistry 210 (2010) 48–53

Contents lists available at ScienceDirect

Journal of Photochemistry and Photobiology A: Chemistry

journal homepage: www.elsevier.com/locate/jphotochem

# A new way to construct luminescent functionalized silicon hybrid material derived from methyldichlorosilane

Haifeng Lu, Hua Wang, Shengyu Feng*

*School of Chemistry and Chemical Engineering, Shandong University, Jinan 250100, PR China*

ARTICLE INFO

*Article history:*
Received 17 September 2009
Received in revised form
16 November 2009
Accepted 11 December 2009
Available online 23 December 2009

*Keywords:*
Methyldichlorosilane
Hydrosilylation reaction
Hybrid material
Lanthanide ion
Photoluminescence

ABSTRACT

The functional precursor (PySi) was derived from the hydrosilylation reaction of methyldichlorosilane and 4-vinylpyridine, and then two series of novel luminescent hybrid materials (RE-PySi, where RE = Tb, Dy) with organic fragments covalently linked to inorganic parts were assembled by a sol–gel process, and characterized by the X-ray diffraction, scanning electron microscopy, and spectroscopy. It is found that the sol–gel treatment has an influence on the organization and microstructure of the hybrid materials, indicating that the hybrid material systems derived from different solvents exhibit different textures. The photoluminescent behavior of these chemically bonded hybrids was studied in detail. The observed green luminescence suggested that the intra-molecular energy-transfer process between the lanthanide ion and the pyridyl group takes place among these molecular-based hybrids.



## 1. Introduction

Luminescent materials have numerous applications, including displays, tunable lasers, amplifiers for communication, and so on [1]. Because of their colorimetric purity, lanthanide ions have been used as basic constituents of luminescent materials, such as illumination lamps, cathode ray tube displays, and optical imaging of cells [2–10]. However, in the past, materials for practical uses were limited to inorganic solids, whereas lanthanide complexes were always excluded just because of their limited thermal stability. Nevertheless, new applications that have been investigated in recent years make such metal complexes an attractive research subject again. The common solution is to link lanthanide complexes to inorganic parts via covalent bonds to generate hybrid materials [11–20].

Because of their excellent stability and mechanical property, silicone- and siloxane-based materials can be employed as versatile hosts, including those based on organic functional groups and transition metals [21,22]. By controlling the conditions of synthesis, the type of templates and the sol–gel treatment, silicone-based particles can be tailored with different shapes, such as nanospheres [22,23], nanorods [24], core–shell particles [25], hollow nanocapsules [26]. Silicone nanomaterials are attracting increasing attention, due to their inherent robustness and tunable physical properties [27,28]. Therefore, development of novel and versatile synthetic methodologies to prepare functionalized silicone nanomaterials that have well-defined shapes and size distributions is highly desirable.

Among all those synthetic routes, there is an one-spot sol–gel methodology in which the tetraalkoxy silane $Si(OR)_4$ and the silane coupling agents $(RO)_3Si(CH_2)_3X$ (where R = Me or Et, X = complexing groups) were mix together to generate multifunctional hybrid materials via simultaneous hydrolysis and condensation reaction in an alcoholic solution in the presence of an acid or a base catalyst [29]. The sol–gel process has been successfully used in the past few years for the production of advanced multi-functional materials such as monoliths, thin films, fibers, and powders [30]. This method is particularly useful in the preparation of nanosized organic/inorganic hybrid composites simply by mixing organic and inorganic components in one pot at around room temperature. However, the synergy of the combination is critical in order to obtain composites exhibiting unusual electrochemical, biological, mechanical, electrical, and optical properties [31,32].

Due to the limitation of the available siloxane coupling agents, modifications of pre-prepared siloxane precursors with the appropriate organic compounds to generate new functional hybrid materials were reported mainly on five paths, that is, amino-modification [13,14,16], carboxylic-modification [15,17], sulfonic-modification [18], sulfide-modification [19] and hydroxyl-modification [20]. Therefore, the design and synthesis of new siloxane precursors will help synthesize versatile expand the multiplicity of the functional hybrid materials.

* Corresponding author. Tel.: +86 531 88364866.
*E-mail address:* fsy@sdu.edu.cn (S. Feng).

1010-6030/$ – see front matter © 2009 Elsevier B.V. All rights reserved.
doi:10.1016/j.jphotochem.2009.12.006

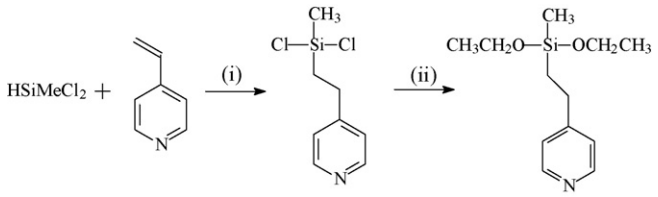


**Scheme 1.** The preparation method of pyridine-functionalized siloxane precursor. (i) $CuCl_2$, N,N,N′,N′-tetramethylethylenediamine, reflux, 16 h. (ii) ethylorthoformate, reflux.

In this paper, we will describe the preparation of luminescent silicon hybrid materials based on tailoring the ternary lanthanide complexes of pyridyl groups. Methyldichlorosilane was chosen as the starting reagent to react first with 4-vinylpyridine by hydrosilylation [33–36], followed by the reaction with the ethylorthoformate to prepare the pyridine-functionalized siloxane precursor. The so-prepared precursor was then utilized to complex with $Dy^{3+}$/$Tb^{3+}$ ions via a sol-gel process to obtain the anticipant hybrid materials. They are generally performed at room temperature where gel particles have to be stabilized by chemical cross-linking. As an alternative, we developed a multi-interphase emulsion process involving the drying gelatine on a vacuum line, followed by the rapid condensation of silicates, leading to stable hybrid microparticles. The structure of the deposited silica particles appears to depend on the process of sol–gel treatment.

## 2. Experimental

### 2.1. Starting materials

Starting materials and solvents were purchased from China National Medicines Group and were distilled before utilization. Europium and terbium nitrates were obtained from their corresponding oxides in dilute nitric acid.

### 2.2. Synthesis of pyridine-functionalized siloxane precursor

The typical procedure for the preparation of pyridine-functionalized siloxane precursor (PySi) was described in Scheme 1 according to the published methods [34,35]. A reaction vessel was charged with 0.2 mole of 4-vinylpyridine, 0.22 mole of methyldichlorosilane, 0.007 mole of N,N,N′,N′-tetramethylethylenediamine and 0.02 mole of cuprous chloride. The resulting mixture was refluxed temperature for 16 h during which the temperature rose from 50 °C to 210 °C. Then 0.32 mole of ethylorthoformate was added to the reaction mixture to replace the silicon-bonded chlorine atoms with ethoxy groups. The resulting mixture was then fractionally distilled to yield pyridine-functionalized siloxane precursor (PySi), which was confirmed by infrared analysis, $^1$H NMR, $^{13}$C NMR and mass spectrum. The boiling point was measured to be 116–124 °C at 1 mm. The yield was approximately 20%. Mass spectra: 240 m/e. $^1$H NMR ($CDCl_3$): $\delta$ 0.10(3H, s, –Si*CH*$_3$), 0.93(2H, m, –Si*CH*$_2$CH$_2$–), 1.19(6H, t, –OCH$_2$*CH*$_3$, $^3J$ = 7 Hz), 2.65(2H, m, –SiCH$_2$*CH*$_2$–), 3.74(4H, q, –O*CH*$_2$CH$_3$, $^3J$ = 7 Hz), 7.1(2H, d, pyridyl, $^3J$ = 5.8 Hz), 8.44(2H, q, pyridyl, $^3J$ = 5.8 Hz). $^{13}$C NMR ($CDCl_3$): $\delta$ −4.9 (–Si*CH*$_3$), 14.6 (–Si*CH*$_2$CH$_2$–), 18(–OCH$_2$*CH*$_3$), 28(–SiCH$_2$*CH*$_2$–), 58(–O*CH*$_2$CH$_3$), 122(pyridyl), 153.5(pyridyl), 149(pyridyl).

### 2.3. Preparation of pyridine-functionalized silicone hybrid materials

0.6 mmol of pyridine-functionalized siloxane precursor (PySi) and 1.2 mmol of tetraethoxysilane (TEOS) were dissolved in 5 mL of ethanol with stirring. Then 1 mL of $CHCl_3$ was added into the solution. The mixture was agitated magnetically in a covered vessel for 1 h to achieve a single phase, followed by the addition of 5 mL of water under gentle stirring for 4 h to form an initial multi-interphase emulsion, which was then dried over a vacuum line at 60 °C immediately. The aging of the mixture lead to the formation of gels (pyridine-functionalized silicone hybrid materials) that were collected for the physical properties studies. All of these hybrids are opaque solid powders and named as PySi-$CHCl_3$. When $CHCl_3$ in the reaction above was substituted by DMF, the hybrid material obtained was named as PySi-DMF.

### 2.4. Preparation of lanthanide ion centered luminescent functionalized silicone hybrid materials

According to the above preparation of pyridine-functionalized silicone hybrid materials, by using 0.2 mmol of $RE(NO_3)_3{\cdot}6H_2O$ (RE = $Dy^{3+}$ and $Tb^{3+}$, respectively), 0.6 mmol of pyridine-functionalized siloxane precursor (PySi) and 1.2 mmol of tetraethoxysilane (TEOS) as starting agent, the lanthanide ion centered luminescent functionalized silicone hybrid materials were prepared. Hybrid material obtained in $CHCl_3$ was named as RE-PySi-$CHCl_3$ while hybrid material obtained in DMF was named as RE-PySi-DMF. Anal. Found for RE-PySi-$CHCl_3$: [$C_{24}H_{33}O_{24}N_6Si_9Tb$] C, 25.0%; H, 4.1%; N, 7.6%; Calcd. for RE-PySi-$CHCl_3$: C, 24.0%; H, 2.8%; N, 7.0%. Anal. Found for RE-PySi-DMF: [$C_{24}H_{33}O_{24}N_6Si_9Tb$] C, 25.0%; H, 4.0%; N, 7.5%; Calcd. for RE-PySi-DMF: C, 24.0%; H, 2.8%; N, 7.0%.

### 2.5. Measurements

Fourier transform infrared (FTIR) spectra were measured within the 4000–400 $cm^{-1}$ region on a Bruker TENSOR27 infrared spectrophotometer with the KBr pellet technique. $^1$H NMR spectra and $^{13}$C NMR spectra were recorded in $CDCl_3$ on a BRUKER AVANCE-400 spectrometer without internal reference. Luminescence (excitation and emission) spectra of solid complexes were determined with a PerkinElmer LS-55 spectrophotometer whose excitation and emission slits were 10 and 5 nm, respectively. The X-ray diffraction (XRD) measurements were carried out on powdered samples via a "BRUKER D8" diffractometer (40 mA 40 kV) using monochromated Cu $K_{\alpha1}$ radiation ($\lambda$ = 1.54 Å) over the 2$\theta$ range of 1–10° and range of 10–70°, respectively. Scanning electronic microscope (SEM) images were obtained with JEOL JSM-7600F.

## 3. Results and discussion

### 3.1. The characterization of the precursor and hybrids

The Fourier Transform Infrared (FTIR) spectra for 4-vinyl pyridine (a), the precursor PySi (b), the Tb-PySi-$CHCl_3$ hybrids (c) and Tb-PySi-DMF hybrids (d) are shown in Fig. 1. In the spectrum (a), the $\nu$(C=C) vibration was observed at 1630 $cm^{-1}$ and the $\nu$(C=C–H) vibration clearly appeared at 2990 $cm^{-1}$ [37]. However, these peaks all disappeared in the curve of the precursor PySi as shown in spectrum (b), indicating that the hydrosilylation reaction has proceeded finished completely and no residual C=C group existed in the precursor PySi. $^1$H NMR, $^{13}$C NMR and mass spectra relative to the precursors are in full agreement with the proposed structure (The data were mentioned above and they could also be found in supplementary material of this paper).

Two adjacent sharp peaks at 2934 and 2886 $cm^{-1}$ in spectrum (b) are $\nu_{as}(CH_2)$ and $\nu_s(CH_2)$ of the long carbon chain in precursors and they could also be observed in the curve of (c) and (d), which proves their existence in the hybrids. The band centered

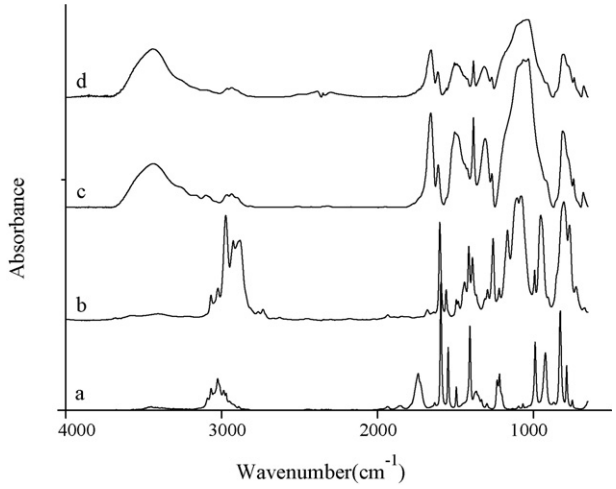


**Fig. 1.** Infrared spectra of 4-vinyl pyridine (a), the precursor PySi (b), the Tb-PySi-$CHCl_3$ hybrids (c) and Tb-PySi-DMF hybrids (d).

at 2982 $cm^{-1}$ in curve of the precursors (b) is the $\nu_s(CH_3)$ in Si-O-$CH_2CH_3$ and Si-$CH_3$ side chains. The $\nu$(Si-O-C) vibration peaks emerged at 1100 and 1076 $cm^{-1}$ in the curve of the precursor PySi (b) turned into a board band at 1031–1110 $cm^{-1}$ of the $\nu$(Si-O-Si) vibration mode in the curve (c) and (d), indicating the completion of hydrolysis and condensation reaction. The $\nu$(O-H) came from the absorbed water in the hybrid material powders.

In the previous research, the comparison between the infrared spectrum of a coordinated pyridine and that of the free base has been used to investigate the coordination process [38–41]. Two changes observed by these investigators are: (1) an upward shift of the four principal bands of pyridine between 1430 and 1600 $cm^{-1}$ (which are due to aromatic C-C and C-N stretching vibrations) and (2) a shift of the ring breathing frequencies and C-H in-plane deformations, which appeared at the 985–1250 $cm^{-1}$ region. The frequencies of the four principal bands of the pyridyl group in the reference [41], the precursor PySi, the Tb-PySi-$CHCl_3$ hybrids and the Tb-PySi-DMF hybrids in the region of 1400–1615 $cm^{-1}$ are listed in Table 1. Because of the dominating (Si-O-Si) absorption bands at 1120–1000 $cm^{-1}$, the two lower frequency bands for these compounds between 985 and 1250 $cm^{-1}$ were too weak to be clearly distinguished; therefore, they are not listed in Table 1.

Comparison of the band shift of these four bands assignment ring C-C and C-N stretching vibrations between the precursor and hybrid materials indicate that the pyridyl group is coordinated to the metal ions. It is well-known that the coordination of pyridyl ring at endocyclic nitrogen lone pairs will increase the wavenumber regarding to the coordination strength [38–40]. Thus it is concluded that ring nitrogen atom is involved in the coordination in the complexes studied.

An ionic nitrate group gives rise to one relatively strong and very sharp combination frequency, while coordinated nitrate groups give two frequencies [42,43]. In these hybrid materials prepared in this paper, the frequency of nitrate group is one relatively strong and sharp at 1658 $cm^{-1}$, so the nitrate group was ionic in the materials.

**Table 1**
The frequencies of the four principal bands respond to the pyridyl group in Ref. [41], the precursor PySi, the Tb-PySi-$CHCl_3$ hybrids and the Tb-PySi-DMF hybrids in the region from 1400 to 1615 $cm^{-1}$.

| Assignment | Ref. [41] | | | This study | | | |
|---|---|---|---|---|---|---|---|
| | 4Apy | M-Ni-4Apy | Δ | Precursor | $CHCl_3$ | DMF | Δ |
| $\nu_{ring}$ | 1602 | 1621 | 19 | 1600 | 1611 | 1612 | 11 |
| $\nu_{ring}$ | 1556 | 1562 | 6 | 1560 | 1559 | 1559 | 1 |
| $\nu_{ring}$ | 1506 | 1524 | 18 | 1494 | 1506 | 1506 | 12 |
| $\nu_{ring}$ | 1440 | 1466 | 26 | 1414 | 1421 | 1422 | 7 |

### 3.2. The photoluminescence of hybrid materials

Fig. 2 is the excitation and emission spectra of the PySi-$CHCl_3$. An excitation band could be found at 320 nm which was attributed to the pyridyl group in the hybrid materials, and a broad emission band centered at 440 nm manifested that the pyridyl group could convert UV light's energy from 320 to 440 nm.

The emission spectra of Tb-PySi-$CHCl_3$ (a), Dy-PySi-$CHCl_3$ (b), Tb-PySi-DMF (c) and Dy-PySi-DMF (d) are shown in Fig. 3. They were obtained by excitating of 320 nm UV light. The emission bands of the terbium materials (curves (a) and (c)) were responded to the transition from the excited state energy level of $Tb^{3+}$ to the different single state levels and were assigned to the $^5D_4 \rightarrow {}^7F_6$ (487 nm) and $^5D_4 \rightarrow {}^7F_5$ (545 nm) transitions. The emission bands of the dysprosium materials (curves (b) and (d)) were attributed to the transition from the excited state energy level of $Dy^{3+}$ to the different single state levels and were assigned to the $^4F_{9/2} \rightarrow {}^6H_{15/2}$ (484 nm) and $^4F_{9/2} \rightarrow {}^6H_{13/2}$ (578 nm) transitions.

Narrow-width green luminescence was observed in the spectra of terbium-containing samples. It should be noted that the green luminescence is not due to the f–f emission of the lanthanide ions alone, but a combination of the blue residual emission of the host matrix in combination with the emission of the lanthanide ions. It is well known that the human eye is sensitive to the monochromatic spectral lights of wavelengths 700 nm (Red), 546.1 nm (Green) and 435.8 nm (Blue) according to the CIE 1931 RGB colorimetric system. These terbium-containing samples (545 nm) have an intrinsic green emission other than the blue background emission of the host matrix. For dysprosium-containing samples, it is a combination of the blue residual emission (440 nm) of host matrix with the yellow emission (484 and 578 nm) of the $Dy^{3+}$ ions.

Comparing the emission spectra in Fig. 2 with Fig. 3, a conclusion could be drawn that the pyridyl groups could absorb the ultraviolet light around 320 nm, lead to emission at 440 nm and transfer the energy to the lanthanide ions via the coordination, and then, lanthanide ions produce luminescence. The antenna effect took place in these systems [44]. However, there are residual emissions of pyridyl groups in the four spectra in Fig. 3, especially in curve (d), which means that the energy transmissions were not completely proceeded. Compared (a) with (b), it is concluded that the energy transmission between pyridyl group and terbium ion is better than that between pyridyl group and dysprosium ion. Compared (a) with (c), it can be concluded that the different synthesis technology of hybrid material could result in the different luminescent performance of the hybrid materials. The differences between two synthetic technologies, one in $CHCl_3$ and the other in DMF, generated the different coordination environment and then influence the luminescent performance. It can be observed from this study that the ethanol–$CHCl_3$–water methodology is better than ethanol–DMF–water one.

### 3.3. The micro-texture and reaction mechanism of hybrid materials

The scanning electron micrographs (SEM) of these hybrid materials can give some characteristics of the texture. Fig. 4 demonstrates that micro-particle materials were obtained. Graphs (a) and (b) respond to Tb-PySi-$CHCl_3$ hybrid materials, and graphs (c) and (d) were obtained from Tb-PySi-DMF hybrid materials. As can be seen in the Graph (a), the Tb-PySi-$CHCl_3$ materials were assembled into irregular nano-particals whose dimensions are about 50–100 nm similar to those of Tb-PySi-DMF materials as shown in

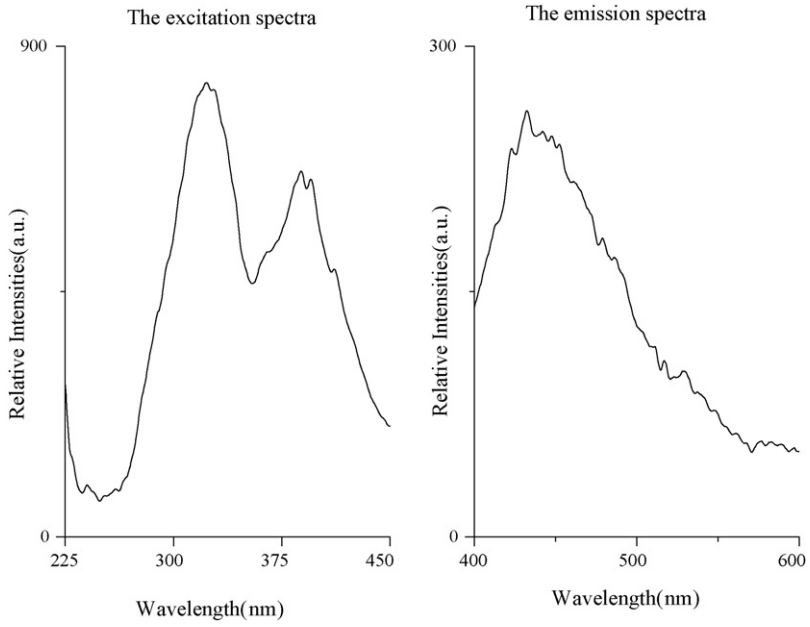


**Fig. 2.** The excitation spectra and emission spectra of PySi-$CHCl_3$.

Graph (c). However, the assembled textures revealed some difference between two kinds of materials. The Tb-PySi-$CHCl_3$ materials have some irregular micro-cavity but the Tb-PySi-DMF materials are massive micro-particles with some edges and planes showing the tendency of crystallization.

To analysis the assembled textures of these two materials, the X-ray diffraction graphs were recorded at $1^\circ \leq n \leq 10^\circ$ and $10^\circ \leq n \leq 70^\circ$ intervals, as shown in Fig. 5. Curve (a) and (5b) responded to Tb-PySi-$CHCl_3$ and Tb-PySi-DMF, respectively. The similarity in XRD graphs proves the similar atom distribution. The diffractogram of hybrid materials with no sharp peak in $10^\circ \leq n \leq 70^\circ$ interval reveals that all these materials are mostly amorphous. They are dominated by a broad peak centered at 23°. It is consistent with the SEM graph of hybrid materials (Fig. 4(a) and (c)). The diffractogram of hybrid materials with no peak at $1^\circ \leq n \leq 10^\circ$ interval reveals that Tb-PySi-$CHCl_3$ (a) and Tb-PySi-DMF (b) have no microporous or mesoporous. However, there are actually some micro-scaled cavities (Fig. 4(b)) and edges (Fig. 4(d)) in the SEM graph. It seems to be conflicted with the SEM graph of hybrid materials. These are mostly due to the sol–gel treatment.

The formation of silica hybrid, in general, involves two major steps: the formation of a wet gel, and drying of the wet gel to

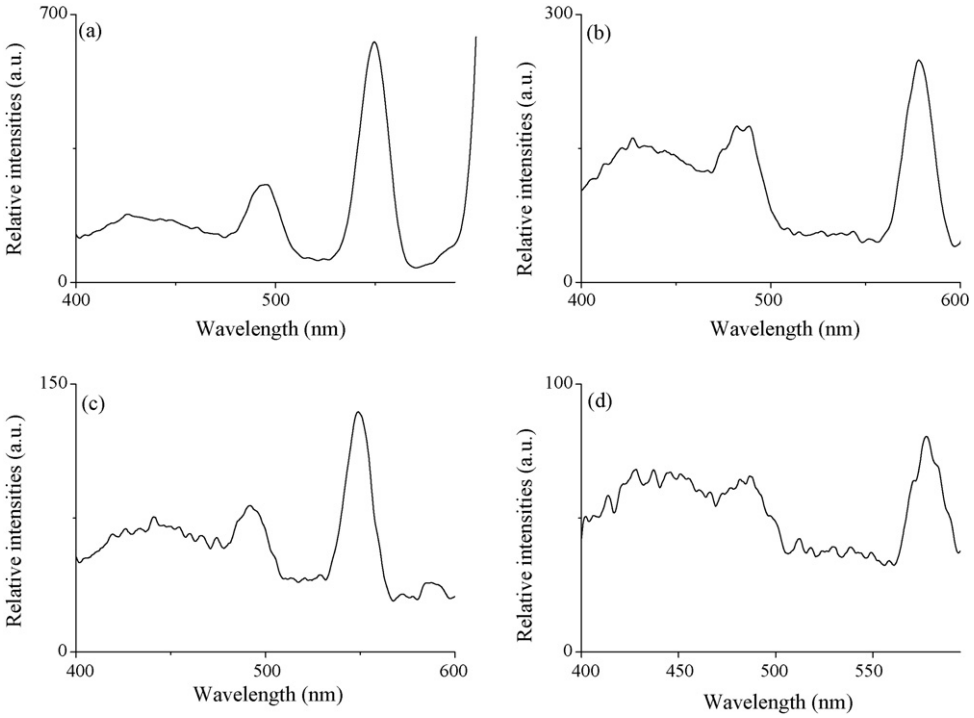


**Fig. 3.** The emission spectra of Tb-PySi-$CHCl_3$ (a), Dy-PySi-$CHCl_3$ (b), Tb-PySi-DMF (c) and Dy-PySi-DMF (d).

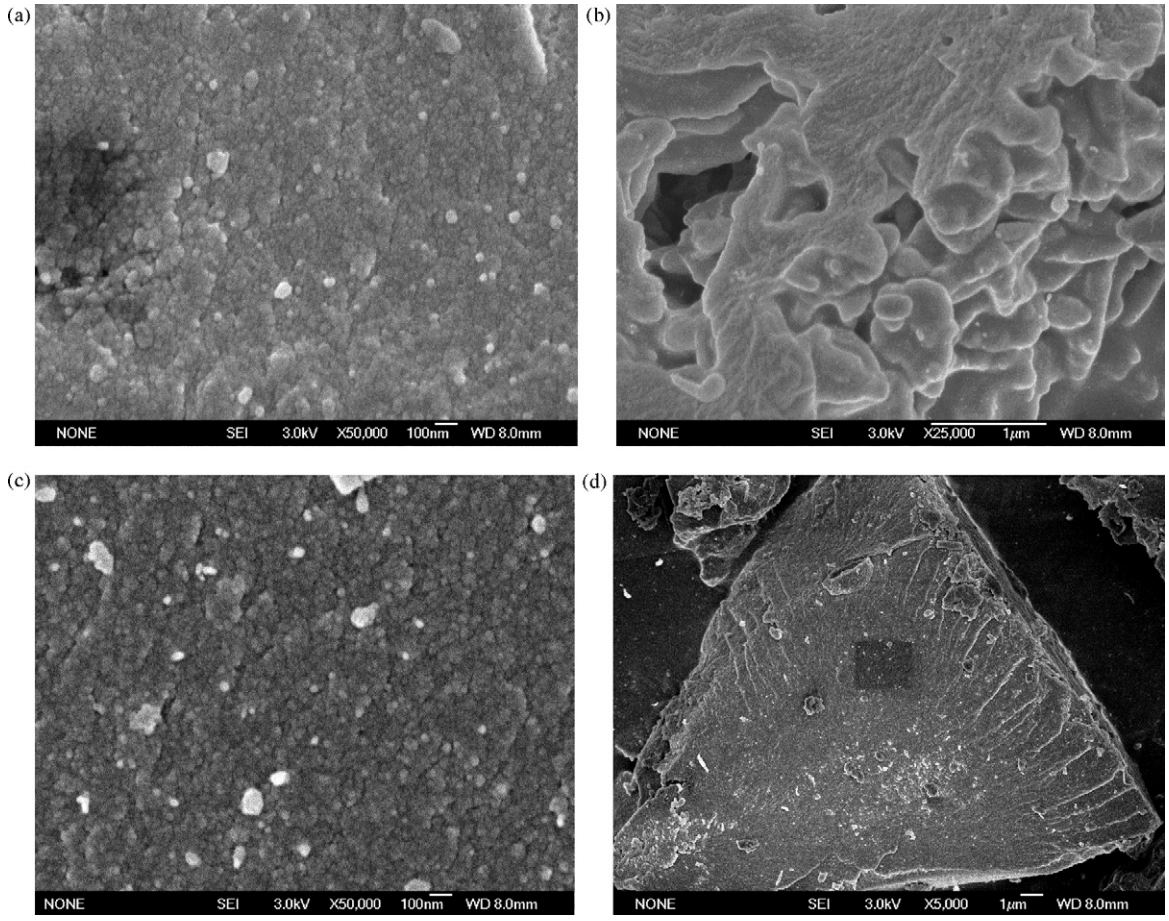


**Fig. 4.** (a)–(d) The scanning electron micrographs (SEM) of hybrid materials.

produce many forms of materials [29–32]. Stable colloidal particles are formed by condensation. The formed structure is controlled by many parameters, such as temperature, the pH of the medium, the nature of the solvent, the water content, the concentration and the drying conditions, etc. [45]. In the sol process, the macro-emulsion is decisive and responsible for the materials' final texture. So the particles of the hybrid materials are about 50–100 nm (Fig. 4(a) and (c)). When the wet gel is dried on a vacuum line at 60 °C, the solvent is evaporated and the gel gets cracked. Because the $CDCl_3$, water and ethanol are very volatile on a vacuum line at 60 °C, the shrinkages of the gel lead to the formation of large pores, supplying the pathways for gas escaping (Fig. 4(b)). As the boiling point of DMF is higher than $CDCl_3$, it leads to a different result. When the gels shrinked step-by-step, the hybrid materials exhibited some edges and planes (Fig. 4(d)) and are denser in structure than those mentioned above.

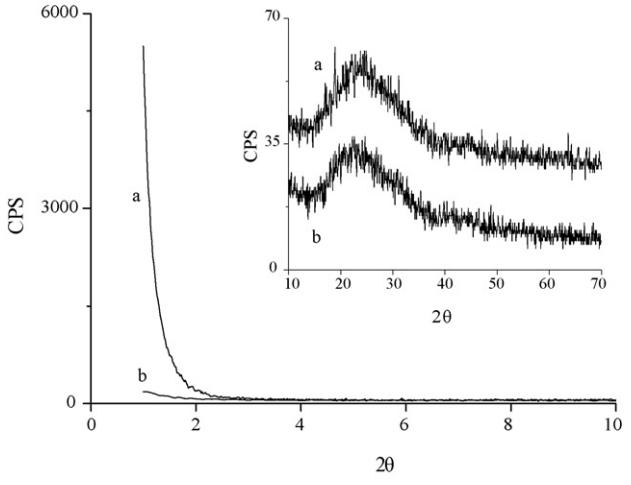


**Fig. 5.** The X-ray diffraction graphs of hybrid materials at $1^\circ \le n \le 10^\circ$ and $10^\circ \le n \le 70^\circ$ intervals. (a) Tb-PySi-$CHCl_3$ and (b) Tb-PySi-DMF.

## 4. Conclusions

In conclusion, we have successfully synthesized two series of novel luminescent hybrid material systems (RE-PySi, where RE = Tb, Dy) by a simple process where the functional precursor was derived from hydrosilylation reaction of methyldichlorosilane with 4-vinylpyridine. The material emits green luminescence by near UV excitation, suggesting that the intra-molecular energy-transfer process between the rare-earth ion and the pyridyl group takes place within these molecular-based hybrids. Because methyldichlorosilane is a convenient starting material for synthesis of various siloxane precursors, the methodology used in this paper could be a promising for tailoring silicone hybrids with desired groups and properties in material in many fields of applications.

More specifically, we report a simple approach to achieving spatially defined organization of colloidal as the main structural motif. They are generally performed at room temperature where gelatine particles have to be stabilized by drying on a vacuum line, leading to stable hybrid micro-texture. The structure of the deposited silica particles appears to depend on the sol–gel treatment; therefore the solvent involved in the system should play an important role in defining the hybrid structures.

## Acknowledgements

This work was supported by the China Postdoctoral Science Foundation Funded Project (20080441135), National Natural Science Foundation of China (20574043 and 20874057) and the Key Natural Science Foundation of Shandong Province of China (No. Z2007B02).

## Appendix A. Supplementary data

Supplementary data associated with this article can be found, in the online version, at doi:10.1016/j.jphotochem.2009.12.006.

## References

[1] G. Blass, B.C. Grabmaier, Luminescent Materials, Springer, Berlin, 1994.
[2] J.G. Bünzli, Benefiting from the unique properties of lanthanide ions, Acc. Chem. Res. 39 (2006) 53–61.
[3] B.M. Tissue, B. Bihari, Lanthanide luminescence as a probe of nanocrystalline materials, J. Fluoresc. 8 (1998) 289–294.
[4] B.M. Tissue, Synthesis and luminescence of lanthanide ions in nanoscale insulating hosts, Chem. Mater. 10 (1998) 2837–2845.
[5] Y. Hasegawa, Y. Wada, S. Yanagida, Strategies for the design of luminescent lanthanide(III) complexes and their photonic applications, J. Photochem. Photobiol. C 5 (2004) 183–202.
[6] E. Terazzi, S. Torelli, G. Bernardineli, J. Rivera, J. Benech, C. Bourgogne, B. Donnio, D. Guillon, D. Imbert, J.G. Bunzli, A. Pinto, D. Jeannerat, C. Piguet, Molecular control of macroscopic cubic, columnar, and lamellar organizations in luminescent lanthanide-containing termotropic liquid crystals, J. Am. Chem. Soc. 127 (2005) 888–903.
[7] P. Lenaerts, K. Driesen, R.V. Deun, K. Binnemans, Covalent coupling of luminescent tris(2-thenoyltrifluoroacetonato) lanthanide(III) complexes on a merrifield resin, Chem. Mater. 17 (2005) 2148–2154.
[8] A.Q. Le Quang, E. Besson, R. Hierle, A. Mehdi, C. Reye, R. Corriu, I. Ledoux-rak, Polymer-based materials for amplification in the telecommunication window: influence of erbium complex concentration on relevant parameters for the elaboration of waveguide amplifiers around 1550 nm, Opt. Mater. 29 (2007) 941–948.
[9] Y. Yang, X. Liu, A. Nakamura, K. Binnemans, J. Liu, Pressure-induced phase transitions on a liquid crystalline europium(III) complex, J. Phys. Chem. B 112 (2008) 5291–5295.
[10] Y.G. Galyametdinov, A.A. Knyazev, V.I. Dzhabarov, T. Cardinaels, K. Driesen, C. Gorlle-walrand, K. Binnemans, Polarized luminescence from aligned samples of nematogenic lanthanide complexes, Adv. Mater. 20 (2008) 252–257.
[11] L.D. Carlos, R.A.S. Ferreira, V. de, Z. Bermudez, S.J.L. Ribeiro, Lanthanide-containing light-emitting organic–inorganic hybrids: a bet on the future, Adv. Mater. 21 (2009) 509–534.
[12] K. Binnemans, Lanthanide-based luminescent hybrid materials, Chem. Rev. 109 (2009) 4283–4374.
[13] K. Binnemans, P. Lenaerts, K. Driesen, C. Görller-Walrand, A luminescent tris(2-thenoyltri-fluoroacetonato) europium(III) complex covalently linked to a 1,10-phenanthroline-functionalised sol–gel glass, J. Mater. Chem. 14 (2004) 191–195.
[14] F.Y. Liu, L.S. Fu, J. Wang, Q.G. Meng, H.R. Li, J.F. Guo, H.J. Zhang, Luminescent film with terbium-complex-bridged polysilsesquioxanes, New J. Chem. 27 (2003) 233–235.
[15] A.C. Franville, D. Zambon, R. Mahiou, Luminescence behavior of sol–gel-derived hybrid materials resulting from covalent grafting of a chromophore unit to different organically modified alkoxysilanes, Chem. Mater. 12 (2000) 428–435.
[16] H.F. Lu, B. Yan, Lanthanide-centered luminescent hybrid micro-sphere particles obtained by sol–gel method, J. Photochem. Photobiol. A: Chem. 194 (2008) 136–142.
[17] B. Yan, K. Qian, H.F. Lu, Molecular assembly and photophysical properties of quatemary molecular hybrid material bond, Photochem. Photobiol. 83 (2007) 1481–1490.
[18] H.F. Lu, B. Yan, Attractive sulfonamide bridging bonds constructing lanthanide centered photoactive covalent hybrids, J. Non-Cryst. Solids 352 (2006) 5331–5336.
[19] B. Yan, H.F. Lu, Lanthanide-centered covalently bonded hybrids through sulfide linkage: molecular assembly, physical characterization, and photoluminescence, Inorg. Chem. 47 (2008) 5601–5611.
[20] H.F. Lu, B. Yan, J.L. Liu, Functionalization of Calix[4]arene as a molecular bridge to assemble luminescent chemically bonded rare-earth hybrid systems, Inorg. Chem. 48 (2009) 3966–3975.
[21] C. Sanchez, F. Ribot, B. Lebeau, Molecular design of hybrid organic–inorganic nanocomposites synthesized via sol–gel chemistry, J. Mater. Chem. 9 (1999) 35–44.
[22] C.A. Bradley, B.D. Yuhas, M.J. Mcmurdo, T.D. Tilley, Functionalized silicone nanospheres: synthesis, transition metal immobilization, and catalytic applications, Chem. Mater. 21 (2009) 174–185.
[23] N. Jungmann, M. Schmidt, M. Maskox, Characterization of polyorganosiloxane nanoparticles in aqueous dispersion by asymmetrical flow field-flow fractionation, Macromolecules 34 (2001) 8347–8353.
[24] V.G. Pol, S.V. Pol, A. Gedanken, S.H. Lim, Z. Zhong, J.J. Lin, Thermal decomposition of commercial silicone oil to produce high yield high surface area SiC nanorods, Phys. Chem. B 110 (2006) 11237–11240.
[25] M. Nakade, T. Ikeda, M. Ogawa, Synthesis and properties of ellipsoidal hematite/silicone core–shell particles, J. Mater. Sci. 42 (2007) 4815–4823.
[26] H. Wang, P. Chen, X. Zheng, Hollow permeable polysiloxane capsules: a novel approach for fabrication, guest encapsulation and morphology studies, J. Mater. Chem. 14 (2004) 1648–1651.
[27] M. Fernandes, V. de Zea Bermudez, R.A. Sá Ferreira, L.D. Carlos, A. Charas, J. Morgado, M.M. Silva, M.J. Smith, Highly photostable luminescent poly(epsilon-caprolactone)siloxane biohybrids doped with europium complexes, Chem. Mater. 19 (2007) 3892–3901.
[28] J. Zou, R.K. Baldwin, K.A. Pettigrew, S.M. Kauzlarich, Solution synthesis of ultrastable luminescent siloxane-coated silicon nanoparticles, Nano Lett. 4 (2004) 1181–1186.
[29] L.S. Fu, Q.G. Meng, H.J. Zhang, S.B. Wang, K.Y. Yang, J.Z. Ni, In situ synthesis of terbium-benzoic acid complex in sol–gel derived silica by a two-step sol–gel method, J. Phys. Chem. Solids 61 (2000) 1877–1881.
[30] U. Schubert, N. Huesing, A. Lorenz, Hybrid inorganic–organic materials by sol–gel processing of organofunctional metal alkoxides, Chem. Mater. 7 (1995) 2010–2027.
[31] C. Sanchez, G.J. de, A.A. Sloer-Illia, F. Ribot, T. Lalot, C.R. Mayer, V. Cabuil, Designed hybrid organic–inorganic nanocomposites from functional nanobuilding blocks, Chem. Mater. 13 (2001) 3061–3083.
[32] K. Damouche, L.D. Carlos, C.V. Santilli, V. de, Z. Bermudez, A.F. Craievich, Small-angle X-ray scattering study of gelation and aging of $Eu^{3+}$-doped sol–gel-derived siloxane-poly(oxyethylene) nanocomposites, J. Phys. Chem. B 106 (2002) 4377–4382.
[33] G.W. Fester, J. Wagler, E. Brendler, U. Böhme, D. Gerlach, E. Kroke, Octahedral $HSiCl_3$ and $HSiCl_2Me$ adducts with pyridines, J. Am. Chem. Soc. 131 (2009) 6855–6864.
[34] B.A. Bluestein, Pyridine Derivatives, United Stated Patent, 3,071,561, 1959.
[35] M. Mazurek, A.M. North, R.A. Pethrick, Synthesis of novel siloxane block copolymers for use in photophysical studies, Polymer 21 (1980) 369–371.
[36] R.A. Abramovitch, D.A. Abramovitch, K. Iyanar, K. Tamareselvy, Application of microwave energy to organic synthesis improved technology, Tetrahedron Lett. 32 (1991) 5251–5254.
[37] E. Pretsch, P. Buhlmann, C. Affolter (Eds.), Structure Determination of Organic Compounds, 2nd printing, Springer, Berlin, 2003.
[38] M. Bakiler, I.V. Maslov, S. Akyuz, Theoretical study of the vibrational spectra of 2-chloropyridine metal complexes. I. Calculation and analysis of the IR spectrum of 2-chloropyridine, J. Mol. Struct. 475 (1999) 83–92.
[39] S. Akyüz, A.B. Dempster, R.L. Morehouse, S. Suzuki, Infrared and Raman Spectroscopic Study of some metal pyridine tetracyanonickelate complexes, J. Mol. Struct. 17 (1973) 105–125.
[40] E. Spinner, The vibration spectra and structures of the hydrochlorides of aminopyridines, J. Chem. Soc. (1962) 3119–3126.
[41] Y. Buyukmurat, S. Akyuz, Theoretical and experimental studies of IR spectra of 4-aminopyridine metal(II) complexes, J. Mol. Struct. 651–653 (2003) 533–539.
[42] N.F. Curtis, Y.M. Curtis, Some nitrato-amine nickel(II) compounds with monodentate and bidentate nitrate ions, Inorg. Chem. 4 (1965) 804–809.
[43] A.B.P. Lever, E. Mantovani, B.S. Ramaswany, Infrared combination frequencies in coordination complexes containing nitrate groups in various coordination environments a probe for the metal–nitrate interaction, Can. J. Chem. 49 (1971) 1957–1964.
[44] G. Crosby, R.E. Whan, R.J. Alire, Intramolecular energy transfer in rare earth chelates role of the triplet state, J. Chem. Phys. 34 (1961) 743–748.
[45] P.C.R. Soares-Santos, H.I.S. Nogueira, V. Felix, M.G.B. Drew, R.A. Sa Ferreira, L.D. Carlos, T. Trindade, Novel lanthanide luminescent materials based on complexes of 3-hydroxypicolinic acid and silica nanoparticles, Chem. Mater. 15 (2003) 100–108.